Polymer 51 (2010) 4398–4407

Contents lists available at ScienceDirect

Polymer

journal homepage: www.elsevier.com/locate/polymer

Structure and properties of polysaccharide nanocrystal-doped supramolecular hydrogels based on Cyclodextrin inclusion

Xiaolan Zhang [a], Jin Huang [a,e,f,*], Peter R. Chang [b,**], Junli Li [a], Yongming Chen [c], Daxin Wang [d], Jiahui Yu [e], Jinghua Chen [g]

[a] College of Chemical Engineering, Wuhan University of Technology, Wuhan 430070, China
[b] Bioproducts and Bioprocesses National Science Program, Agriculture and Agri-Food Canada, 107 Science Place, Saskatoon, SK S7N 0X2, Canada
[c] Beijing National Laboratory for Molecular Science, Division Polymer Science and Materials, Institute of Chemistry, Chinese Academy of Science, Beijing 100190, China
[d] Subei People's Hospital of Jiangsu Province, Yangzhou University, Yangzhou 225001, China
[e] Interdisciplinary Science and Technology Institute for Advanced Study, East China Normal University, Shanghai 200062, China
[f] State Key Laboratory of Pulp and Paper Engineering, South China University of Technology, Guangzhou 510640, China
[g] School of Medicine and Pharmaceutics, Jiangnan University, Wuxi 214122, China

ARTICLE INFO

Article history:
Received 16 January 2010
Received in revised form
10 July 2010
Accepted 18 July 2010
Available online 24 July 2010

Keywords:
Supramolecular hydrogel
Cyclodextrin inclusion
Polysaccharide nanocrystal

ABSTRACT

Polysaccharide nanocrystals, such as the rod-like whiskers of cellulose and chitin, and platelet-like starch nanocrystals, were for the first time incorporated into supramolecular hydrogels based on cyclodextrin/polymer inclusion in order to enhance mechanical strength and regulate drug release behavior. The structures and properties of the resultant nanocomposite hydrogels were characterized by X-ray diffraction (XRD), scanning electron microscopy (SEM) and rheological testing. As expected, the elastic modulus of the nanocomposite hydrogels climbed, owing to the reinforcing function of the polysaccharide nanocrystals. The modulus of the cellulose whisker-doped hydrogel was 50 times higher than that of the native hydrogel. Furthermore, the presence of polysaccharide nanocrystals increased the stability of the hydrogel framework and inhibited the diffusion of bovine serum albumin, which served as a model protein drug in the nanocomposite hydrogels and showed prominent sustained release profiles. Importantly, the incorporation of polysaccharide nanocrystals did not show additional cytotoxicity as comparison with the native hydrogel. In addition, the inherited shear-thinning property of the nanocomposite hydrogels contributed to their potential as injectable biomaterials.

1. Introduction

Born out of the growing interest in the predominant properties attributed to nanoparticles, novel bionanocrystals derived from natural polysaccharide has attracted great attention owing to their distinct biocompatibility and biodegradability [1]. These bionanocrystals are crystalline residues with a uniform structure acquired through acidic or alkaline hydrolysis of natural polysaccharides. The alternatives are so called rod-like whiskers of cellulose [2] and chitin [3], and platelet-like starch nanocrystal [4]. Similar to traditional inorganic nanoparticles, these polysaccharide nanocrystals also exhibit high specific strength and modulus (i.e. high rigidity), a high specific active surface area, and hence contribute a reinforcing function to the as-prepared nanocomposites [1,2,5]. Additionally, the surfaces of polysaccharide nanocrystals are covered with a number of hydroxyl groups, which make it convenient to perform chemical and/or physical conjugation between polysaccharide nanocrystals and the polymer matrix [6,7]. Currently, academic research and practical application of polysaccharide nanocrystals concentrates mainly on environmentally friendly materials because of their biodegradability and reinforcing function [1,2,5]. As far as we know, a study on the application of these polysaccharide nanocrystals to reinforcing biomaterials by virtue of their biocompatibility, which is higher than most inorganic nanoparticles, has not yet been reported.

Supramolecular hydrogels, based on cyclodextrin (CD)/polymer inclusion, as one of the promising biomaterials, have sparked great interest [8–16]. The formation of such supramolecular hydrogels generally consists of two stages: firstly, the CD host threads onto the guest polymer chain to form polyrotaxane (PR), which is stabilized by the host-guest hydrophobic interactions and hydrogen bonding among the CDs [17–19]. The subsequent spontaneous aggregation of

* Corresponding author. College of Chemical Engineering, Wuhan University of Technology, 122 Loushi Road, Wuhan 430070, China. Tel.: +86 27 63373510; fax: +86 27 87859019.
** Corresponding author.
E-mail addresses: huangjin@iccas.ac.cn (J. Huang), peter.chang@agr.gc.ca (P.R. Chang).

0032-3861/$ – see front matter © 2010 Elsevier Ltd. All rights reserved.
doi:10.1016/j.polymer.2010.07.025

the PRs plays a role in the physical crosslinking that drives gelation [8–16,20–27]. In some cases, the hydrophobic aggregation of the uncovered segments also acts as a physical crosslink to improve the formation of the hydrogels [11,12,14,15,24–27]. Such supramolecular hydrogels can encapsulate cells [15,16] and drugs [10–15] *in situ* during the gelation process. It not only facilitates enhancing drug loading-levels, but also avoids the structural changes for the drug and the interference of cell activity caused by chemical crosslinking. This advantage of physical encapsulation is prominent particularly in the drug categories of proteins, peptides, and nucleic acids. On the other hand, the host-guest recognition of CD/polymer and non-covalent aggregation of PRs contribute to a reversible sol–gel transition as a function of temperature [8,10,14,20–24] and shearing [8–15,24–26]. These stimulus-response properties provide great potential as injectable biomaterials [8,10,12–14], and break though the limits of the conventional implantable strategy for hydrogels. Furthermore, the temperature sensitivity may also provide the intelligence required for drug delivery and release [10,12,14].

Recently, in order to improve hydrogel performance by incorporating nanofiller [28–30], the work on supramolecular hybrid and nanocomposite hydrogels based on CD/polymer inclusion has been performed [31–35]. In many cases, the incorporated nanoparticles not only accelerated gelation [31,33], but also regulated the mechanical performance of the hydrogels [33]. Remarkably, the functions of the nanoparticles were inherited by the as-prepared hybrid and nanocomposite hydrogels. For example, incorporated Fe_3O_4 nanoparticles endowed the nanocomposite hydrogels with a superparamagnetic effect [33] while the hybrid hydrogels containing Ag nanoparticles possessed good catalytic activity [34], both of which may be beneficial for extending the application of these supramolecular hydrogels. However, for supramolecular hydrogels made using PEO-*b*-PPO-*b*-PEO polymer, the addition of carbon nanoparticles, such as single-walled carbon nanotube [31] and graphene sheet [35], reduced the mechanical strength in spite of shortening gelation time. This resulted from the absence of micellization of the hydrophobic poly(propylene oxide) (PPO) block in the PEO-*b*-PPO-*b*-PEO polymer as another physical crosslink [26] when the PPO block interacted with the incorporated carbon nanoparticles to stabilize them in aqueous media. In addition, the *in situ* formed Ag nanoparticles in the aqueous PEO-*b*-PPO-*b*-PEO polymer solution prolonged the gelation process induced by the CD inclusion and decreased the mechanical strength of the as-prepared hybrid hydrogel [34].

As mentioned above, polysaccharide nanocrystals exhibit a polar surface covered with numerous hydroxyl groups and their reinforcing role has been verified in many nanocomposite systems [1,2,5]. As a result, polysaccharide nanocrystals of various compositions and structures, such as cellulose whisker (CW), chitin whisker (CHW) and starch nanocrystal (StN), were expected to reinforce the supramolecular hydrogels based on α-CD and the PEO_{137}-*b*-PPO_{44}-*b*-PEO_{137} polymer and, meanwhile, shorten the gelation process. The "channel-type" crystallinity of the PR aggregation (as a main supporting framework of hydrogels) was characterized by X-ray diffraction (XRD), while the inner morphologies of the hydrogels were observed by scanning electron microscope (SEM). The shear-thinning, drug release and temperature sensitivity properties of the as-prepared nanocomposite hydrogels were also investigated for use as potential injectable smart biomaterials.

2. Experimental part

2.1. Materials

The triblock polymer of PEO_{137}-*b*-PPO_{44}-*b*-PEO_{137} (EPE) (M_n = 14600, PEO content = 82.5 wt%) and α-Cyclodextrin (α-CD), as well as dimethyl sulfoxide (DMSO) and 3-[4,5-Dimethylthiazol-2-yl]-2,5-diphenyl tetrazolium bromide (MTT), were purchased from Aldrich. The linter was kindly supplied by Hubei Chemical Fiber Co. Ltd. (Xiangfan, China). The crab shell chitin was supplied by Ocean and Biochemical Co. Ltd. (Yuhuan, China). The pea starch, with an average size around 30 μm and composed of 35 wt% amylose and 65 wt% amylopectin, was supplied by Nutri Pea Co. Ltd. (Portage la Prairie, Canada). All other reagents were of analytical grade and commercially sourced in China.

2.2. Extraction of polysaccharide nanocrystals

Cellulose whisker (CW) from linter was prepared using the procedure reported by Azizi-Samir et al. [36] with minor modifications. 20 g of linter was dispersed into 175 mL of 30% (v/v) H_2SO_4, and then stirred at a speed of 100 rpm for 6 h at 60 °C. The resultant suspension was washed with distilled water by successive centrifugation until approximate neutrality. Subsequently, a small amount of 5 wt% ammonia was added, and then dialyzed with distilled water. Finally, lyophilization was used to obtain CW in a powder form. The TEM image in Fig. 1(A) shows that the length and diameter of the rod-like CW dispersed in water were ca. 250 nm and 10 nm, respectively.

Crab shell chitin whisker (CHW) was prepared using the procedure reported by Nair et al. [3]. Crab shell chitin was first boiled and stirred in a 5 wt% KOH solution for 6 h to remove most of the proteins. It was then kept at ambient temperature overnight with stirring, followed by filtration and washing several times with distilled water. The resultant chitin sample was bleached with 17 g of $NaClO_2$ in 1 L 0.3 M sodium acetate buffer for 6 h at 80 °C, and was then kept in a 5% KOH solution for 48 h to remove residual proteins. After centrifuging at 3600 rpm for 15 min, the purified chitin was collected, and further hydrolyzed with boiling 3 M HCl for 90 min under stirring to produce a chitin whisker suspension. Herein, 1 g of purified chitin corresponded to 30 mL of 3 M HCl. The resultant acid hydrolyzed chitin whisker suspension was collected by centrifugation at 3600 rpm for 15 min, dialyzed in running water for 2 h, and then dialyzed overnight in distilled water. Finally, lyophilization was used to obtain the CHW in powder form. The TEM image in Fig. 1(B) shows that the length and diameter of the rod-like CHW dispersed in water were ca. 200 nm and 15 nm, respectively.

Pea starch nanocrystal (StN) was prepared using the procedure reported by Angellier et al. [4]. 14.69 g of pea starch was dispersed into 100 mL of 3.16 M H_2SO_4, and then stirred at a speed of 100 rpm for 5 days at 40 °C. The resultant suspension was washed with distilled water by successive centrifugation until approximate neutrality. Finally, lyophilization was used to obtain StN in a powder form. The TEM image in Fig. 1(C) shows the StNs dispersed in water tended to self-aggregate. The individual StN marked by arrows was observed to have a platelet shape similar to the previous report [4] with a width of ca. 10–20 nm and length of ca. 40–70 nm.

2.3. Preparation of nanocomposite hydrogels

Firstly, 600 mg freeze-dried polysaccharide nanocrystal powder was dispersed into 20 mL of deionized water using ultrasonic treatment. Because some aggregated agglomerates were difficult to dismantle, the suspension was centrifuged at 4000 rpm for 20 min and the upper aqueous suspension was collected. Meanwhile, the precipitate was dried under vacuum and weighed to determine the polysaccharide nanocrystal content in the upper aqueous suspension. Herein, the CW, CHW and StN were used respectively. Subsequently, α-CD was dissolved in water to form a transparent solution after heat treatment. At the same time, the EPE was

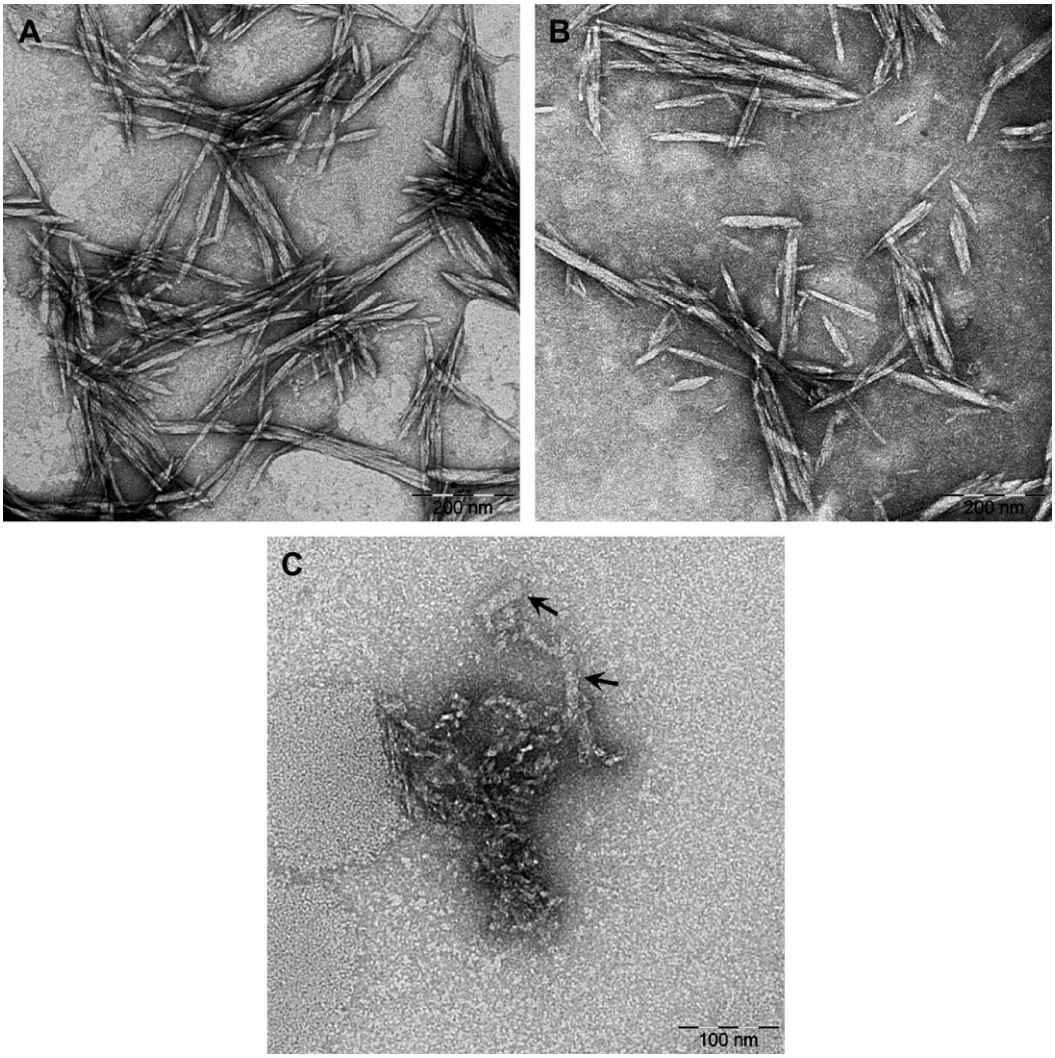

Fig. 1. TEM images of polysaccharide nanocrystals dispersed in water – rod-like CW (A) and CHW (B), and platelet-like StN (C).

dissolved in the aqueous polysaccharide nanocrystal suspension, and vigorously stirred. The α-CD aqueous solution was then added to the aqueous suspension containing EPE and polysaccharide nanocrystals. After a 2 min ultrasonic treatment, the mixture was conditioned at ambient temperature for gelation. The ultimate concentrations of α-CD and EPE in the mixture were fixed at 90 mg mL^{-1} and 10 mg mL^{-1}, respectively. In the nanocomposite hydrogels, the loading-levels of CW and CHW in the whole solid varied as 0.1, 0.5, 1.0, 2.5 wt%; however, the loading-levels of StN were limited to below 0.5 wt%, i.e. 0.1 and 0.5 wt%, because the self-aggregation of StN in aqueous media, shown in Fig. 1(C), resulted in sedimentation during the gelation period. The nanocomposite hydrogels were coded as EPE/CD/CW-number, EPE/CD/CHW-number and EPE/CD/StN-number, according to the type and loading-level of polysaccharide nanocrystals. In these codes, the number was the weight percentage of the polysaccharide nanocrystals. In addition, a native hydrogel containing only α-CD and EPE was prepared for comparison.

2.4. Characterization

Transmission electron microscopy (TEM) was carried out on an H-7000FA transmission electron microscope (Hitachi, Japan) at an acceleration voltage of 75 kV. Deposited CW, CHW and StN were negatively stained with an aqueous 2% solution of uranyl acetate before being observed and photographed.

Scanning electronic microscopy (SEM) was carried out on an S-3000 N scanning electron microscope (Hitachi, Japan) with an acceleration voltage of 20 kV. The nanocomposite and native hydrogels were individually freeze-dried onto silicon wafers, and then coated with gold for observation and being photographed.

X-ray diffraction (XRD) measurements of the freeze-dried polysaccharide nanocrystal powders and the nanocomposite and native hydrogels were carried out on a D/max-250 X-ray diffractometer (Rigaku Denki, Japan) equipped with a Cu Kα radiation source ($\lambda = 0.154$ nm). The diffraction data were collected over a range of $2\theta = 5–60^\circ$ using a fixed time mode with a step interval of 0.02°.

The changes in viscosity of nanocomposite sols containing various levels of polysaccharide nanocrystals, as well as of the native EPE/CD hydrogel, were traced by an NDJ-79 rotational viscometer (Electromechanical Factory of Tongji University, China) at a constant temperature.

The rheological behavior of the nanocomposite and native hydrogels were measured on an ARES-RFS III rheometer (TA Instruments, USA) using a parallel plate geometry with a diameter of 50 mm. The gap distance between the two plates was fixed at 1 mm. A frequency sweep test was conducted on each sample to

determine values for the storage modulus (G') and loss modulus (G'') over a frequency (ω) range of 0.1–100 rad s^{-1} at 25 °C. The steady flow behaviors were performed over a shearing rate range of 0.01–50 s^{-1}. Dynamic strain sweep measurements were carried out at 1 rad s^{-1} to determine the linear viscoelastic regime over a strain range of 0.1–100%. Temperature control was established by a Julabo FS 18 cooling/heating bath kept within ±0.5 °C over an extended period of time.

2.5. In vitro drug release studies

Bovine serum albumin (BSA), as a model macromolecular protein drug, was used to investigate the effect of polysaccharide nanocrystals on the release profiles of supramolecular hydrogels. Except for phosphate buffered saline solution (pH = 7.4) (PBS) as the aqueous media and the addition of 6.0 mg BSA ($M_n = 67{,}000$) vs. 81 mg α-CD, the preparations for drug-loaded nanocomposite and native hydrogels were similar to the process mentioned above. The entire mixture, with a volume of 0.9 mL, was poured into a 1 mL cuvette and incubated in a 37 °C water bath for 1 h until gelation. For *in vitro* release studies, the cuvette with the hydrogel was placed in a test tube containing 12 mL PBS, and then conditioned in a shaking table at 37 °C. After a given interval, 0.5 mL buffer medium was removed to determine the absorbance at 595 nm on a UV-1900PC spectroscope (Shanghai, China), and hence calculate the concentration of released BSA. At the same time, the same volume of fresh PBS solution was added to keep the total solution volume constant.

2.6. Cell viability assays

Mouse muscular cell line L929 was supplied from Institute of Biochemistry & Cell Biology, Chinese Academy of Sciences. Cells were cultured in RPMI 1640 (Gibco BRL, Paris, France), supplemented with 10% fetal bovine serum (FBS, HyClone, Logan, Utah), streptomycin at 100 μg mL^{-1}, and penicillin at 100 U mL^{-1}. All cells were incubated at 37 °C in a humidified 5% CO_2 atmosphere. Cells were splited by using trypsin/EDTA solution when almost confluent.

A total of 2 g of each hydrogel sample was put into 10 mL of RPMI 1640 cell culture medium in a 15 mL centrifuge tube and placed in a shaker incubator (37 °C, 60 rpm) for 2 days. After that, the medium was filtered with a 0.22 μm sterile filter into a sterile container and stored in a refrigerator at 4 °C before use.

L929 cells were seeded into 96 well plates at an initial density of 1×10^4 cells per well in 100 μL RPMI 1640 growth medium and incubated for 18–20 h to reach 80% confluency at the time of treatment. Cell culture medium was replaced by 100 μL of the extracted leached medium from the corresponding hybrid hydrogels. After 48 h incubation, the well was washed twice with PBS solution. A total of 10 μL of MTT solution (5 mg mL^{-1} in PBS) was added to each well. Plates were incubated for 4 h in a CO_2 cell culture incubator, MTT solution was removed, and 100 μL of DMSO was added to each well. Plates were incubated for 10 min in the incubator, and then for 15 min at room temperature. The optical density (OD) at 570 nm was measured using an automatic BIO-TEK microplate reader (Powerwave XS, USA) to evaluate the metabolic activity of the cells. Cell viability was calculated from the following equation:

$$\text{Cell viability}\left(\%\right) = \frac{\text{OD}_{\text{sample}}}{\text{OD}_{\text{control}}} \times 100\%$$

where OD_{sample} represented the OD value from a well treated with sample and $OD_{control}$ from a well treated with PBS buffer only. Each experiment was carried out in triplicate. Results were shown as means and corresponding standard deviations (mean ± SD).

3. Results and discussion

3.1. Formation of nanocomposite hydrogels

As shown in Fig. 2, the cellulose whisker (CW)-doped nanocomposite sols with loading-levels of 0.5 wt% and 0.1 wt% and the native EPE/CD sol were selected as the representatives for tracing the apparent state evolvement. The nanocomposite sol containing 0.5 wt% CW lost flowability in ca. 45 min while the immobility of the sol containing the lower 0.1 wt% loading-level occurred after another ca. 5 min. At this time, the mixture of only EPE and α-CD was still a viscous sol. The immobility time of native EPE/CD sol required ca. 70 min. The presence of CW obviously accelerated the gelation of supramolecular hydrogels based on EPE and α-CD. Changes in the viscosity during gelation of nanocomposite sols containing various loading-levels of three polysaccharide nanocrystals, as well as the native EPE/CD sol, further verified the role of polysaccharide nanocrystals in accelerating the gelation. As shown in Fig. 3(A and B), the viscosities of nanocomposite sols containing CW and CHW dramatically increased over time, and were obviously higher than the native EPE/CD sol at the same interval. This increased viscosity resulted in a loss of flowability of the sols because a hydrogel formed. In this work, the gelation viscosity of the EPE/CD sol was consistent with the previous report [31], i.e. gelation occurred when the viscosity reached ca. 300 cP. As a result, the dependence of viscosity upon time (Fig. 3) could be used to predict the gelation time of the nanocomposite sols containing polysaccharide nanocrystals more accurately than a visual observation of flowability could. Furthermore, with an increase in the CW and CHW loading-levels, the extent of viscosity increase of nanocomposites was higher at the same time interval, indicating that higher loading-levels of polysaccharide nanocrystals could shorten the gelation time. As reported [26], gelation of the EPE/α-CD mixing solution was driven by two kinds of physical cross-linking, i.e. the "channel-type" crystallization of the inclusion complex based on poly(ethylene oxide) (PEO)/α-CD, and micellization of the middle hydrophobic poly(propylene oxide) (PPO) blocks. With regards to the nanocomposite hydrogels loaded with CW and CHW, two positive factors for improving the gelation formation may be considered: (i) the polysaccharide nanocrystals

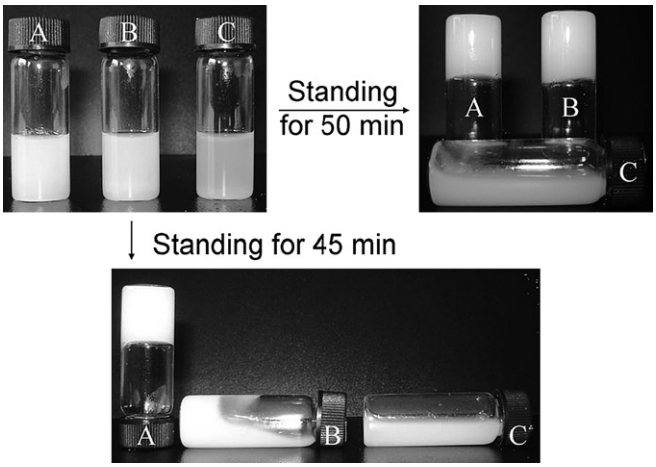

Fig. 2. Apparent state evolvement of the CW-doped nanocomposite sols with loading-levels of 0.5 wt% (A) and 0.1 wt% (B) as the representatives, and the native EPE/CD sol (C) for comparison.

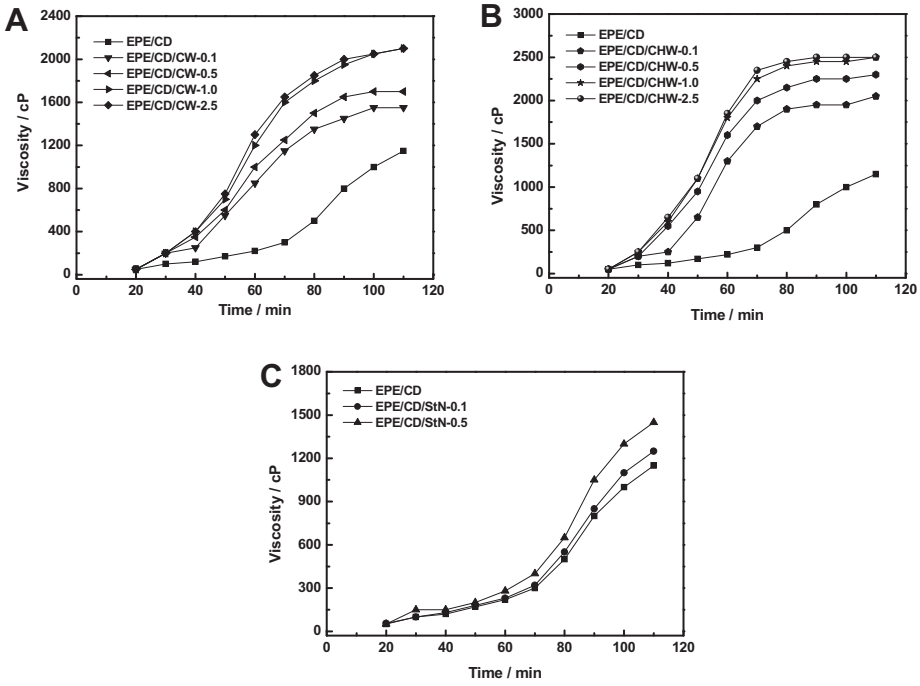

Fig. 3. Comparison of the kinetics of nanocomposite hydrogels containing three polysaccharide nanocrystals (A for CW, B for CHW and C for StN) with various loading-levels, as well as the native EPE/CD hydrogel.

had a nucleation effect inducing crystallization of the PEO/α-CD polyrotaxanes; and (ii) the polar hydroxyl groups on the surface of polysaccharide nanocrystals may be hydrogen bonded with the hydrogel matrix to produce a new physical crosslink. However, as shown in Fig. 3(C), the viscosities of nanocomposite hydrogels containing starch nanocrystal (StN) increased slowly and reached a gelation viscosity of ca. 300 cP at ca. 70 min, indicating that a loading-level of lower than 0.5 wt% StN had almost no effect on shortening gelation time in comparison with the native hydrogel. This may be ascribed to the self-aggregation of StN to some extent inhibiting the two positive factors of improving gelation mentioned above. As in previous reports [8,10,14,20–24], these nanocomposite hydrogels, that were constructed by many kinds of physical interactions, showed temperature sensitivity, meaning that the physical joints gradually cleaved with elevating temperature. Herein, the nanocomposite hydrogels conditioned at ambient temperature became sols at ca. 66 °C with a heating rate of 2 °C min^{-1}.

3.2. Structure and morphology of nanocomposite hydrogels

Fig. 4 shows the XRD patterns of the freeze-dried powders of the native EPE/CD hydrogel and the nanocomposite hydrogels with different loading-levels of various polysaccharide nanocrystals, and the freeze-dried CW, CHW, StN, EPE and α-CD powders for

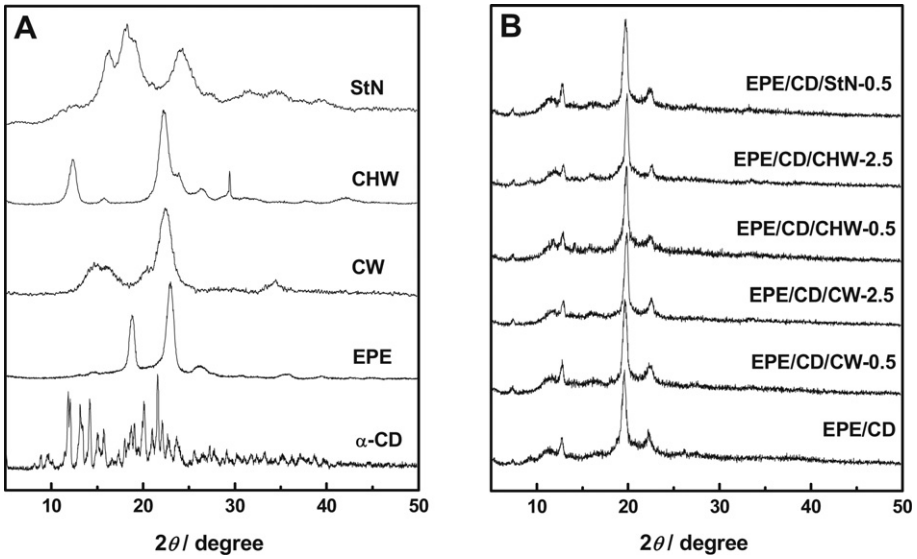

Fig. 4. X-ray patterns of the freeze-dried CW, CHW and StN powders as well as neat EPE and α-CD powders (A), and of the nanocomposite hydrogels containing various polysaccharide nanocrystals at various loading-levels as well as the native EPE/CD hydrogel (B).

comparison. The XRD patterns of all the freeze-dried hydrogels were distinctly different from that of α-CD, and showed a characteristic peak of the "channel-type" crystallinity based on ordered stacking of PEO/α-CD polyrotaxanes [8–27,31–35] located at 2θ of 19.4°. This verified that ordered stacking of the PEO/α-CD polyrotaxanes played a role in forming physical joints for constructing the hydrogel network. In addition, the patterns of the nanocomposite hydrogels were similar to those of the native EPE/CD hydrogel. The absence of the crystallinity characteristic of polysaccharide nanocrystals was ascribed to the low loading-level and to the relatively weak diffraction intensity.

The SEM images in Fig. 5 show the inner morphologies of the freeze-dried native EPE/CD hydrogel and nanocomposite hydrogels with different loading-levels of various polysaccharide nanocrystals. All of the hydrogels exhibited a loose sponge-like structure, a characteristic of a crosslinked network. This porous structure resulted from the leakage or evaporation of the trapped water molecules during the freeze-drying process. With an increase in the CW and CHW loading-levels, the pore size of the nanocomposite hydrogels showed a tendency to increase, while the wall thickness of the supporting framework also gradually increased. The nanocomposite hydrogels containing StN showed a distinct morphology with a relatively smoother fractured surface and less interconnection.

3.3. Mechanical reinforcement of nanocomposite hydrogels

Fig. 6 depicts the dynamic rheological behaviors of the native EPE/CD hydrogel and of the nanocomposite hydrogels with different polysaccharide nanocrystals and loading-levels. The storage modulus (G') of all the native and nanocomposite hydrogels exhibited a substantial elastic response, which was greater than the loss modulus (G'') over the entire range of the measuring frequency. This suggested that these supramolecular hydrogels possessed a permanent network, in spite of physical interaction as the stabilizing force, and hence displayed strength and rigidity.

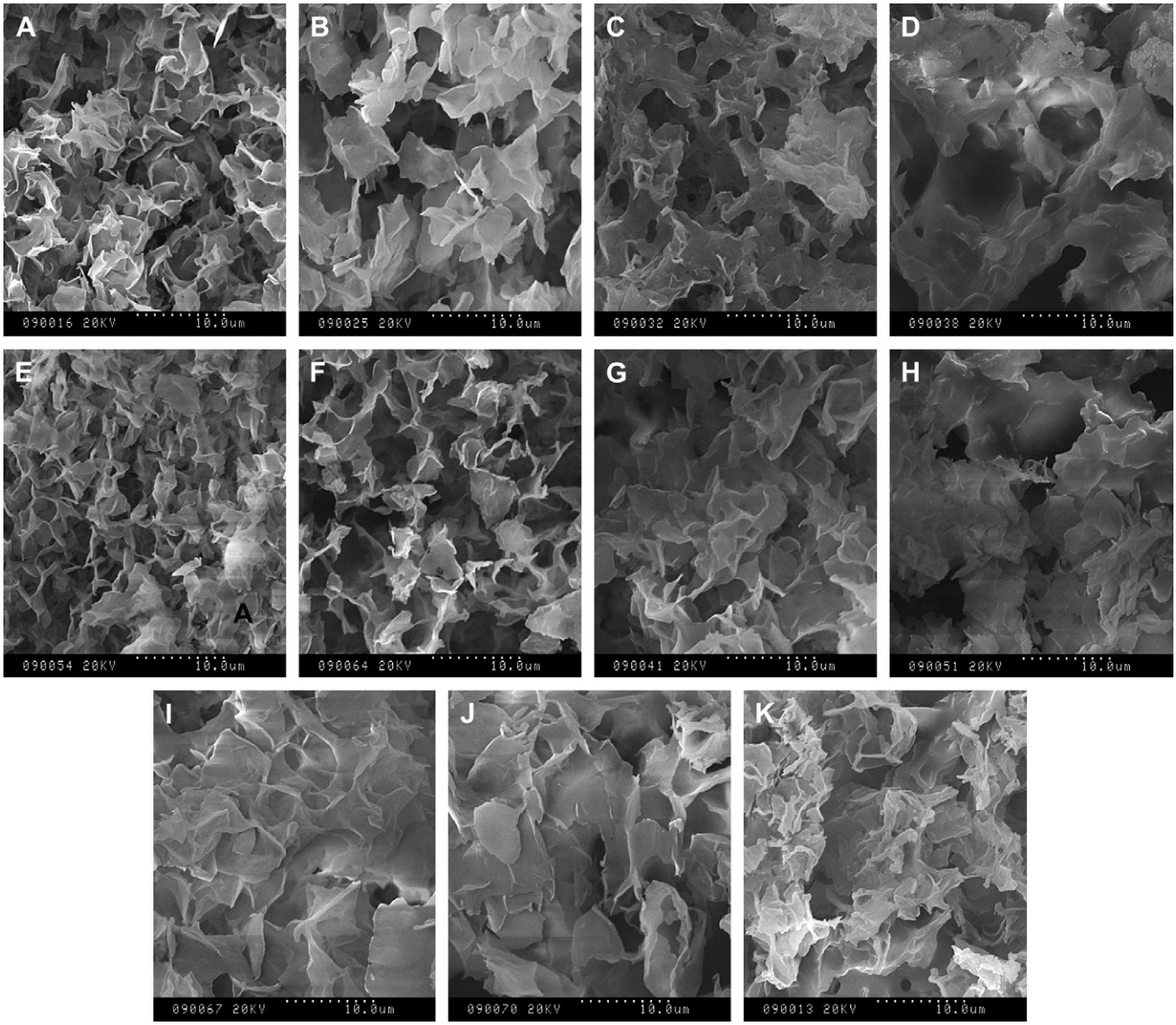

Fig. 5. SEM images of the freeze-dried nanocomposite hydrogels EPE/CD/CW-0.1 (A), EPE/CD/CW-0.5 (B), EPE/CD/CW-1.0 (C), EPE/CD/CW-2.5 (D), EPE/CD/CHW-0.1 (E), EPE/CD/CHW-0.5(F), EPE/CD/CHW-1.0 (G), EPE/CD/CHW-2.5 (H), EPE/CD/StN-0.1 (I) and EPE/CD/StN-0.5 (J), and the freeze-dried native EPE/CD hydrogel for comparison (K).

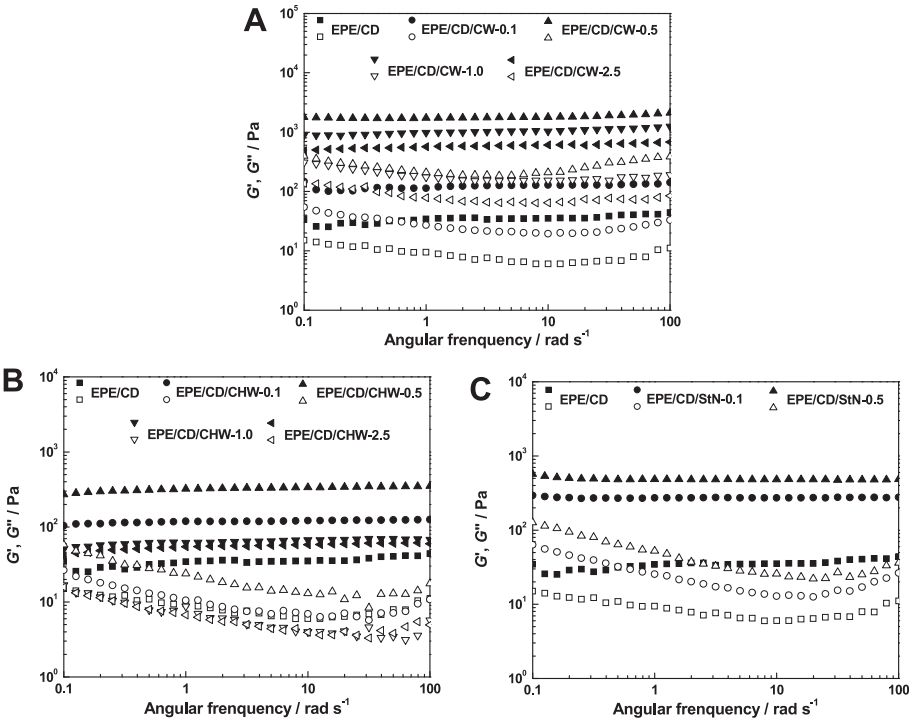

Fig. 6. Dynamic rheological behavior of the nanocomposite hydrogels containing various loading-levels of CW (A), CHW (B) and StN (C), as well as the native EPE/CD hydrogel for comparison. (Solid symbols for storage modulus, G', and hollow symbols for loss modulus, G'').

Furthermore, except for the slight downward shift of the G'' curves for the nanocomposite hydrogels with greater than 1.0 wt% CHW, the incorporation of polysaccharide nanocrystals resulted in an upward shift of the G' and G'' curves, indicating that the polysaccharide nanocrystal-doped nanocomposite hydrogels exhibited higher G' values. Consequently, the mechanical reinforcing function of the polysaccharide nanocrystals was verified. It was ascribed to an improvement in crystallization due to

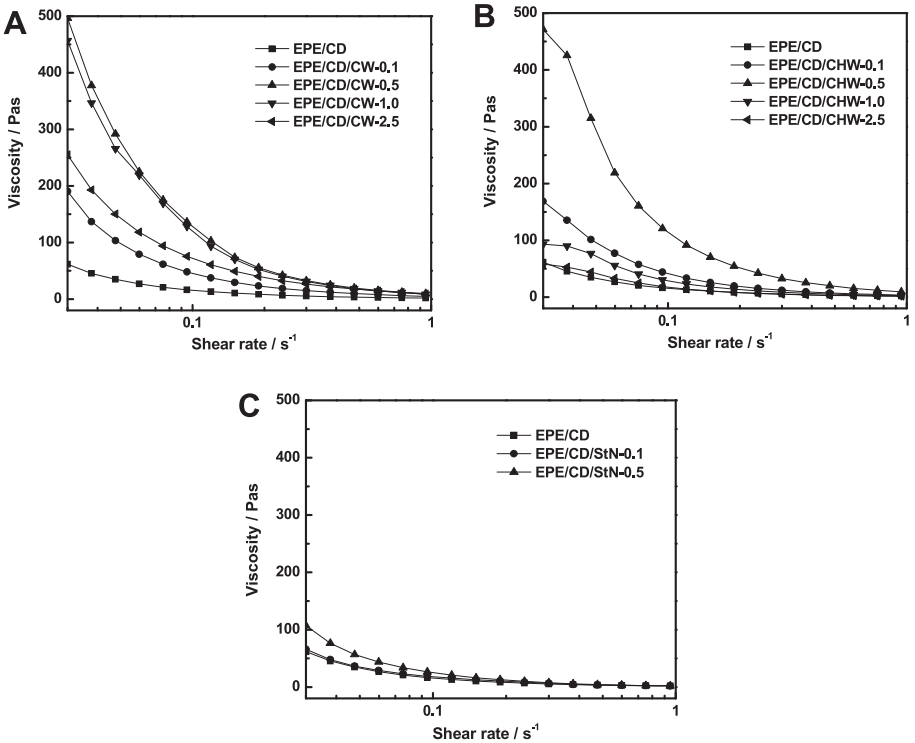

Fig. 7. Steady rheological behavior of the nanocomposite hydrogels containing various loading-levels of CW (A), CHW (B) and StN (C), as well as the native EPE/CD hydrogel for comparison.

a nucleation effect of polysaccharide nanocrystals, and to an increased physical crosslinking acted by hydrogen bonding between incorporated polysaccharide nanocrystals and hydrogel matrix.

Both the type and loading-level of the polysaccharide nanocrystals were the factors that regulated the G' and G'' values of the nanocomposite hydrogels. With an increase in the loading-level of polysaccharide nanocrystals up to 0.5 wt%, the G' values initially increased. However, when the loading-level of polysaccharide nanocrystals was higher than 1.0 wt%, the G' values decreased for the nanocomposite hydrogels containing CW and CHW with an increase in the loading-level of polysaccharide nanocrystals. At this time, the decrease of the G' values at higher loading-levels was attributed to the increasing aggregation of the polysaccharide nanocrystals. Furthermore, the loading-level of 0.5 wt%, which produced the highest mechanical strength in the nanocomposite hydrogels doped with the same polysaccharide nanocrystal, was taken as the example to investigate the effect of the polysaccharide nanocrystal categories on the mechanical reinforcement. The nanocomposite hydrogels loaded with 0.5 wt% polysaccharide nanocrystals were ranked according to their G' values in the order of EPE/CD/CW-0.5 > EPE/CD/CHW-0.5 > EPE/CD/StN-0.5. It was worth noting that the EPE/CD/CW-0.5 nanocomposite hydrogel had the maximum G' value ca. 1700, which was ca. 50 times higher than that of the native EPE/CD hydrogel. The CW avoided protonation of amino groups on the CHW surface and the self-aggregation of StN, which inhibited hydrogen bonding between polysaccharide nanocrystals and hydrogel matrix.

3.4. Shear-thinning properties of hydrogels

Fig. 7 depicts the steady rheological behavior of the native EPE/CD hydrogel and nanocomposite hydrogels with various loading-levels and types of polysaccharide nanocrystals. With an increase in shearing rate, the viscosity of all the native and nanocomposite hydrogels diminished greatly until, at a shearing rate of 1 s^{-1}, the viscosities were close to that of the native EPE/CD hydrogel. This indicated that the polysaccharide nanocrystal-doped nanocomposite hydrogels inherited the supramolecular characteristic of the native EPE/CD hydrogel. Incorporation of the polysaccharide nanocrystals enhanced the initial viscosity in comparison with that of the native EPE/CD hydrogel. Furthermore, the dependence of the initial viscosity upon the polysaccharide nanocrystal loading-level was similar to that of the G' value, namely the initial viscosity increased until the 0.5 wt% loading-level followed by a decline in initial viscosity for the nanocomposite hydrogels loaded with higher than 1.0 wt% of CW or CHW. As a result, nanocomposite hydrogels containing 0.5 wt% CW and CHW exhibited the maximum initial viscosities in the two systems. The decrease in initial viscosity at loading-levels higher than 1.0 wt% was ascribed to the self-aggregation of CW and CHW. Similarly, the easy aggregation of StN inhibited the association between the StN filler and the hydrogel matrix, resulting in only a very small increase in the initial viscosity of the StN-doped nanocomposite hydrogels. When the shearing force was removed, the flowable sols recovered the same as the hydrogels did. Such reversible gel–sol transition induced by shearing is a key for an injectable biomaterial.

3.5. In vitro release profiles of hydrogels

Bovine serum albumin (BSA) as a model protein drug was encapsulated in the hydrogels to investigate *in vitro* release kinetics. Fig. 8 shows the dependence of the cumulative release ratio upon the type of polysaccharide nanocrystals (A) and on the CW loading-level (B). The release profiles of all the tested BSA-loaded hydrogels showed a sustained release characteristic. The release process of the nanocomposite hydrogels lagged in contrast to that of the native EPE/CD hydrogel. The native EPE/CD hydrogel released almost all of the encapsulated BSA in 18 days because the hydrogel was completely eroded by solution; however, the cumulative release rate for the nanocomposite hydrogels was only ca. 80% after 20 days. Consequently, the incorporation of polysaccharide nanocrystals facilitated the sustained release of the drug. When the polysaccharide nanocrystal loading-level was 0.5 wt%, the cumulative release ratio at a given time was in the order as follows: EPE/CD/CW-0.5 < EPE/CD/CHW-0.5 < EPE/CD/StN-0.5. At the same time, for nanocomposite hydrogels with various levels of CW, the cumulative release ratio at a given time first decreased as the loading-level increased up to 0.5 wt%, and then increased with a continuous increase of the CW loading-level.

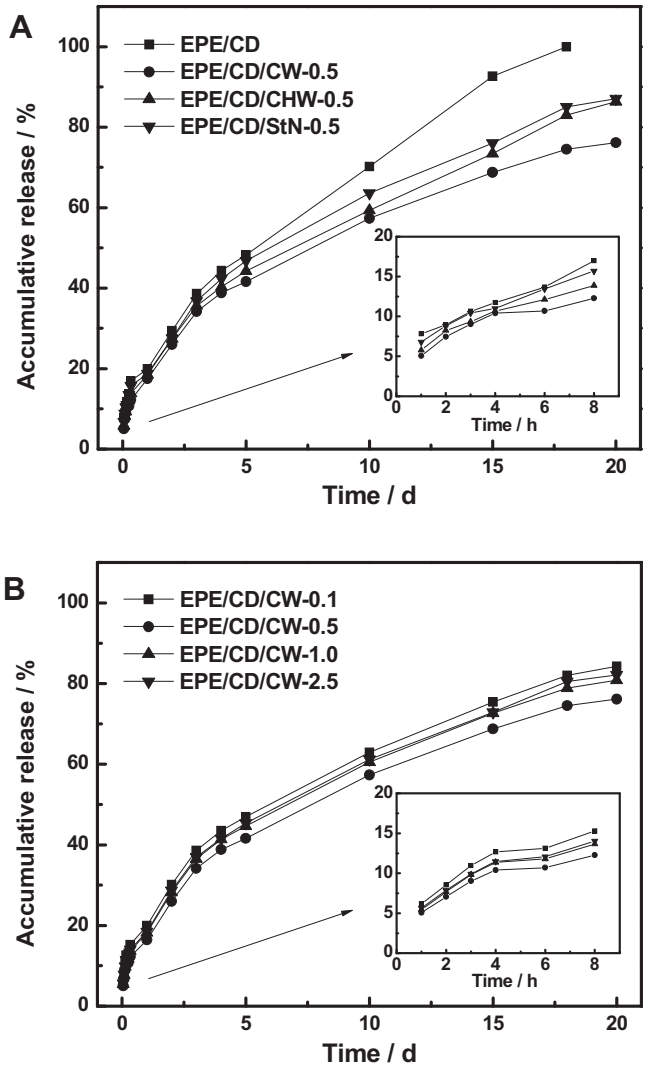

Fig. 8. *In vitro* release profiles for BSA from native EPE/CD hydrogel and nanocomposite hydrogels containing 0.5 wt% polysaccharide nanocrystals – EPE/CD/CW-0.5, EPE/CD/CHW-0.5 and EPE/CD/StN-0.5 (A); nanocomposite hydrogels of EPE/CD/CW containing various loading-levels of CW (B).

It was observed that the hydrogel volume gradually decreased as the incubation time increased; as a result, the drug release was ascribed mainly to the erosion of hydrogel at the interface between hydrogel exterior and solution. The positive factors that led to acceleration of gelation and improved mechanical strength, i.e. nucleation of polysaccharide nanocrystals to induce crystallization

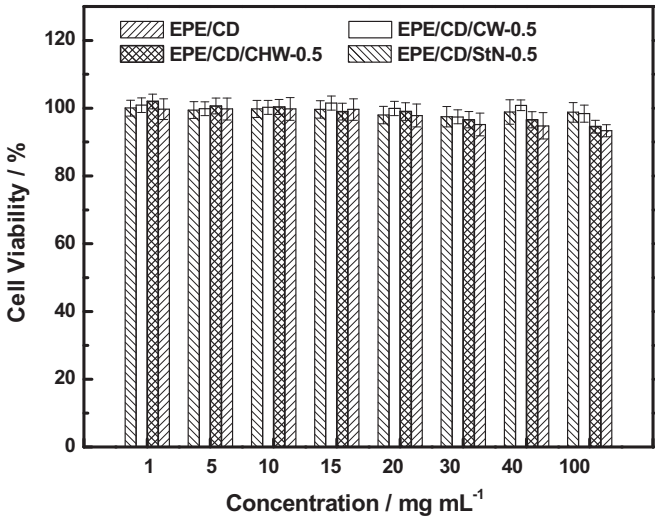

Fig. 9. *In vitro* cell viability after 48 h in the extracted media leached from nanocomposite and native hydrogels of various concentrations.

of the PEO/α-CD PRs and hydrogen bonding between polysaccharide nanocrystals and hydrogel matrix as physical crosslinking, also resisted the erosion of the hydrogel exterior immersed into solution and the diffusion of external solution into hydrogel, and hence maintained the stability of the hydrogel framework. On the other hand, release of encapsulated drug from the hydrogels was also under control of diffusion. SEM observations (Fig. 5) showed that the nanocomposite hydrogels loaded with greater than 1.0 wt% CW and CHW had larger inner cavities which facilitated the diffusion and release of the encapsulated BSA. At this time, the polar surface of the polysaccharide nanocrystals may play a role in immobilizing the encapsulated BSA by intermolecular interaction, and hence slow the drug release. In order to clarify the drug release mechanism, the release kinetics of the drug was simulated by the Peppas equation. In the initial 8 h, the index (n) of time in the Peppas equation was calculated to be lower than 0.45. This could be assigned to Fickian diffusion, namely the release mechanism was mainly ascribed to the drug diffusion; however, after 1 day, the drug release was in accordance with non-Fickian diffusion because the index (n) value of time in the Peppas equation was in the range of 045–0.89. At this time, besides drug diffusion, erosion of the hydrogel framework cooperatively determined the drug release behavior as well.

3.6. Cytotoxicity of nanocomposite hydrogels

The predominant advantages of polysaccharide nanocrystals are their biocompatibility and biodegradability. Combined with the good sustained release profile, injection potential, and temperature sensitivity, the polysaccharide nanocrystal-doped supramolecular nanocomposite hydrogels may be considered as a kind of injectable smart biomaterial. As a result, in order to investigate the effect of the incorporated polysaccharide nanocrystals on cytotoxicity, the *in vitro* cell viability of the extracted leached media from the corresponding nanocomposite and native hydrogels was evaluated by the MTT method using the L929 cell line. Fig. 9 shows the cell viability of the solid component in the nanocomposite and native hydrogels *in vitro* at 48 h. The results showed that the cell viability of all the nanocomposite and native hydrogels was close to 100%, and verified that incorporation of polysaccharide nanocrystals did not increase the cytotoxicity of the nanocomposite materials even when the concentration reached 100 mg mL^{-1}.

4. Conclusions

Biocompatible and biodegradable polysaccharide nanocrystals were first introduced into the systems of supramolecular hydrogels based on cyclodextrin/polymer inclusion. A notable fact is that the incorporation of polysaccharide nanocrystals showed many advantages, such as accelerating gelation, enhancing mechanical strength, improving erosion resistance of solution, and facilitating long term sustained release of drugs. The results showed that the cellulose whisker and the 0.5 wt% loading-level were the optimal conditions which gave the highest storage modulus and the shortest gelation time. In addition, the polysaccharide nanocrystal-doped supramolecular nanocomposite hydrogels inherited shear-thinning and temperature sensitivity properties which contribute to the potential for injection-implantation method, smart delivery and controlled release. Furthermore, cell viability evaluation verified that the incorporation of polysaccharide nanocrystals did not produce additional cytotoxicity in supramolecular nanocomposite hydrogels which is fundamental to the application of such nanocomposite hydrogels in the biomedical field. Consequently, polysaccharide nanocrystal-doped supramolecular nanocomposite hydrogels seem to be a good candidate for a controlled system for drug delivery and release with an injection-implantation function. As far as we know, this work is the first significative attempt at using the biocompatible and biodegradable polysaccharide nanocrystals in the nanocomposite biomaterials, and shows the positive effect.

Acknowledgements

The research work was financially supported by the National Natural Science Foundation of China (20404014, 50873080 and 50843031); 973 Projects of Chinese Ministry of Science and Technology (2007CB936104 and 2009CB930300); Program of Energy Research and Development (PERD) of Canada; Agricultural Bioproducts Innovation Program (ABIP) of Canada via the Pulse Research Network (PURENET); Shanghai Municipality Commission for Special Project of Nanometer Science and Technology (0952nm05300); Shanghai Municipality Commission for International Corporation Project (10410710000) and for Non-Governmental International Corporation Project (09540709000); Foundation for New Century Excellent Talents in University of Ministry of Education of China (NCET-10-0435); Youth Chenguang Program of Science & Technology in Wuhan (200850731383); State Key Laboratory of Pulp and Paper Engineering (200906); and Fundamental Research Funds for the Central Universities (Self-Determined and Innovative Research Funds of WUT 2010-II-022 and JUSRT30905).

References

[1] Dufresne AJ. Nanosci Nanotechnol 2006;6:322.
[2] Azizi-Samir MAS, Alloin F, Dufresne A. Biomacromolecules 2005;6:612.
[3] Nair KG, Dufresne A. Biomacromolecules 2003;4:657.
[4] Angellier H, Choisnard L, Molina-Boisseau S, Ozil P, Dufresne A. Biomacromolecules 2004;5:1545.
[5] Dufresne A. Can J Chem 2008;86:484.
[6] Chen GJ, Wei M, Chen JH, Huang J, Dufresne A, Chang PR. Polymer 2008;49:1860.
[7] Cao X, Habibi Y, Lucia LA. J Mater Chem 2009;19:7137.
[8] Li J. Adv Polym Sci 2009;222:79.
[9] Van de Manakker F, Vermonden T, van Nostrum CF, Hennink WE. Biomacromolecules 2009;10:3157.
[10] Li J, Loh XJ. Adv Drug Deliv Rev 2008;60:1000.
[11] Li X, Li J. J Biomed Mater Res A 2008;86A:1055.
[12] Li J, Li X, Ni XP, Wang X, Li HZ, Leong KW. Biomaterials 2006;27:4132.
[13] Li J, Ni X, Leong KW. J Biomed Mater Res A 2003;65A:196.
[14] Ren LX, He LH, Sun TC, Dong X, Chen YM, Huang J, et al. Macromol Biosci 2009;9:902.

[15] Wu DQ, Wang T, Lu B, Xu XD, Cheng S, Jiang XJ, et al. Langmuir 2008;24:10306.
[16] Wang T, Jiang XJ, Tang QZ, Li XY, Lin T, Wub DQ, et al. Acta Biomaterialia 2009;5:2939.
[17] Wenz G, Han BH, Müller A. Chem Rev 2006;106:782.
[18] Huang F, Gibson HW. Prog Polym Sci 2005;30:982.
[19] Miyake K, Yasuda S, Harada A, Sumaoka J, Komiyama M, Shigekawa H. J Am Chem Soc 2003;125:5080.
[20] Huh KM, Cho YW, Chung H, Kwon IC, Jeong SY, Ooya T, et al. Macromol Biosci 2004;4:92.
[21] Choi HS, Kontani K, Huh KM, Sasaki S, Ooya T, Lee WK, et al. Macromol Biosci 2002;2:298.
[22] Choi HS, Yamamoto K, Ooya T, Yui N. ChemPhysChem 2005;6:1081.
[23] He LH, Huang J, Chen YM, Xu XJ, Liu LP. Macromolecules 2005;38:3845.
[24] Zhao SP, Zhang LM, Ma D. J Phys Chem B 2006;110:16503.
[25] Zhao SP, Zhang LM, Ma D. J Phys Chem B 2006;110:12225.
[26] Li J, Li X, Zhou Z, Ni X, Leong KW. Macromolecules 2001;34:7236.
[27] Yuan RX, Shuai XT. J Polym Sci Part B Polym Phys 2008;46:782.
[28] Hu X, Xiong L, Wang T, Lin Z, Liu X, Tong Z. Polymer 2009;50:1933.
[29] Zhang Y-T, Zhi T-T, Zhang L, Huang H, Chen H-L. Polymer 2009;50:5693.
[30] Xiong L, Hu X, Liu X, Tong Z. Polymer 2008;49:5064.
[31] Wang ZM, Chen YM. Macromolecules 2007;40:3402.
[32] Guo M, Jiang M, Pispas S, Yu W, Zhou C. Macromolecules 2008;41:9744.
[33] Ma D, Zhang LM. J Phys Chem B 2008;112:6315.
[34] Ma D, Xie X, Zhang LM. J Polym Sci Part B Polym Phys 2009;47:740.
[35] Zhu SZ, Han BH. J Phys Chem C 2009;113:13651.
[36] Azizi-Samir MAS, Alloin F, Sanchez JY, El Kissi M, Dufresne A. Macromolecules 2004;37:1386.